



# A design of air flow configuration for cooling lithium ion battery in hybrid electric vehicles



Heesung Park\*

Research & Development Division, Hyundai Motor Company, Republic of Korea

## HIGHLIGHTS

- Air cooled battery system was optimized by numerical simulations.
- The cooling performance was investigated by thermal resistance model.
- Required cooling performance was achieved by tapered manifold with air ventilation.

## ARTICLE INFO

### Article history:

Received 31 December 2012

Received in revised form

28 February 2013

Accepted 4 March 2013

Available online 27 March 2013

### Keywords:

Air cooling

Lithium ion battery

Electric vehicle

Hybrid electric vehicle

## ABSTRACT

Lithium ion batteries are commonly employed in hybrid electric vehicles and achieving high energy density in the battery has been among the most critical issues in the automotive industry. Since thermal management is very important in the automotive batteries with layout limitation, a design strategy for effective cooling should be carefully opted. Particularly, a forced air cooling has been considered as a practical option in the automotive industry. In this article, a specific design of air-cooled battery system is theoretically investigated and numerically modelled to satisfy the required thermal specifications. Since a typical battery system in hybrid electric vehicles consists of the stacked multiple battery cells, cooling performance is determined mainly by the uniform distribution of air flow in the coolant passage which dissipates heat generated from the battery cells. It is demonstrated that the required cooling performance can be achieved by employing the tapered manifold and pressure relief ventilation even without changing the layout/design of the existing battery system. Furthermore, a theoretical analysis is performed as a design guideline to enhance the cooling performance.

© 2013 Elsevier B.V. All rights reserved.

## 1. Introduction

Hybrid electric vehicles (HEVs) are expected to provide long-range driving and reasonable refuelling time at the affordable price ranges which is strongly demanded by the modern drivers of full-function passenger vehicles. For such vehicles, the high-voltage battery system is indispensable for driving performance since the battery provides electric power to the driving motor when accelerating and is charged from driving motor during regenerative braking periods. Therefore, the batteries themselves need to accommodate high electrical currents [1] over many charging–discharging cycles. In order to achieve sufficiently high voltages to power HEVs, many cells must be connected in series to create a battery system that will likely be confined to an internal compartment within the vehicle [2]. Thus, high energy density is a

critical factor in the HEV battery for the guaranteed long driving ranges and reasonable vehicle sizes. For this, various redox chemistries and electrolyte materials have been investigated to optimize the energy density in the battery cell [3]. In conventional lithium ion batteries, organic electrolyte solutions consisting of organic solvents, which exhibit flammability and volatility, are used [4]. Although high energy density in the battery system is unavoidable to commercialize HEVs, safety and long-term durability became significant issues [5] due to potential overheating [6] or thermal runaway under extreme conditions [7–9]. Therefore, a well-designed cooling system is an essential part in the HEV battery [10] to safely maintain the battery temperature under the required conditions. Moreover, the life span of lithium ion battery cell is reduced by about two months for every degree of temperature rise in an operating range of 30–40 °C [11]. The battery system is required to maintain the maximum temperature below 40 °C and the battery cell temperature difference below 5 °C for a full lifespan [12].

\* Tel.: +82 10 2690 3461.

E-mail address: [heros93@gmail.com](mailto:heros93@gmail.com).

In this regard, the battery thermal management system, including traditional cooling systems, such as an air-based thermal management system with an electric fan [1,7,11,13], a liquid-based thermal management system [14,15] cooled with water, glycol, oil, acetone or even refrigerants, a heat pipe-based thermal management system [16] and a PCM thermal management system [6,17] have been investigated by many researchers [18]. Heat generation and dissipation rates have been simulated under natural and forced air convection conditions [7]. The optimum values for the flow resistance coefficient of battery system were obtained for enhancing heat dissipation with a given cooling fan. Wu et al. [19] suggested that the forced convection cooling with heat pipe could be effective to control the temperature in the battery. The passive thermal management system with phase change material has been introduced to achieve efficient cooling of the battery system in stressful conditions [6,17]. Giuliano et al. [2] measured the various temperatures with thermochromic liquid crystal during charging and discharging conditions. They proposed a mechanism that the uneven heat generation causes a temperature gradient across the face of the cell. Reciprocated air flow for cooling was designed by Mahamud and Park [11] to improve temperature uniformity and reduce maximum cell temperature. Karimi and Li [13] proposed that another cooling strategy based on the distributive forced-convection is an efficient and cost-effective method that can achieve the uniformity in both temperature and voltage distributions within the battery pack at the various discharge rates.

Many advanced cooling schemes have been proposed for effective thermal management in the HEV battery system, however, the air-cooled battery system is still dominant due to the manufacturing cost, parasitic energy loss, full battery system weight, and layout limitation. Additionally, air ventilation is necessary in the particular battery systems which produce potentially hazardous gases [18,20,21]. In this report, a forced-air cooling technique for Li-ion battery system in HEV is introduced within the given design constraints. Numerical simulation is conducted to predict the air flow distribution in the coolant passages and the temperature distribution in the battery system. It is shown that the maximum temperature in the battery system can be successfully controlled under the necessary thermal specifications with a proposed design of tapered manifold and pressure relief ventilation.

## 2. Design for the air flow configuration

The battery system for the HEVs is composed of 72 battery cells in two rows to operate 270 V and 1400 Wh. The coolant passages

(3 mm) are formed between the battery cells to dissipate heat flux of  $245 \text{ W m}^{-2}$  from battery cells (Fig. 1). In a row, 36 battery cells and 37 coolant passages are installed. The overall dimension of the battery system is  $225 \text{ mm} \times 191 \text{ mm} \times 787 \text{ mm}$  in width, height and length, respectively. The configurations of the cooling air flows are displayed in Fig. 2. The heights of the inlet and outlet manifolds are 20 mm for each and the dimension of a coolant passage is  $3 \text{ mm} \times 65 \text{ mm} \times 151 \text{ mm}$ . In the HEV application, the followings are the design constraints of the air cooling system.

- Thermal design specification: the maximum temperature difference between the cell and inlet air is below  $20^\circ\text{C}$ .
- Air flow rate: maximum flow rate is  $0.045 \text{ m}^3 \text{ s}^{-1}$ . Characteristic curves of fan are shown in Fig. 3.
- Inlet and outlet regions should be located on the same side.
- The heights of the inlet and outlet manifolds are below 20 mm.
- The pressure drop should be minimized to operate the fan with the lowest power consumption.

Due to the layout limitation of the battery system in the HEVs, both the inlet and outlet should be located on the same side. Since the distribution of air flow rate for the coolant passages directly affects the temperature of the battery system, optimum manifold design is critical. In this regard, five types of the manifolds are designed and displayed in Fig. 4. Type I has the rectangular-shaped manifold whereas type II and III have the tapered manifolds in the vertical direction that are linearly expanded or contracted from 20 mm to 10 mm and vice versa. Note that type IV is considered for the purpose of comparison. For type V, a rectangular ventilation hole is added to type III in the outlet manifold.

## 3. Numerical calculation

Numerical calculations are conducted to investigate the effect of manifold design on the temperature distribution. Commercially available three-dimensionally computerized fluid dynamics code (Star ccm + version 7.02) is used in this study. In the numerical analysis, the energy and  $k-\epsilon$  turbulent models are employed while buoyancy is neglected. The Reynolds numbers ( $\text{Re} = \text{velocity} \times \text{characteristic length} \times \text{kinematic viscosity}^{-1}$ ) are 28,900 at the inlet and below 2000 at the coolant passages. Incompressible air is assumed and all the calculation results are presented at the steady state condition. Polyhedral type with prism layer is used to generate mesh in the computational domain. The total number of meshes is about 2,400,000 elements as shown Fig. 2(c). Mass flow inlet and pressure

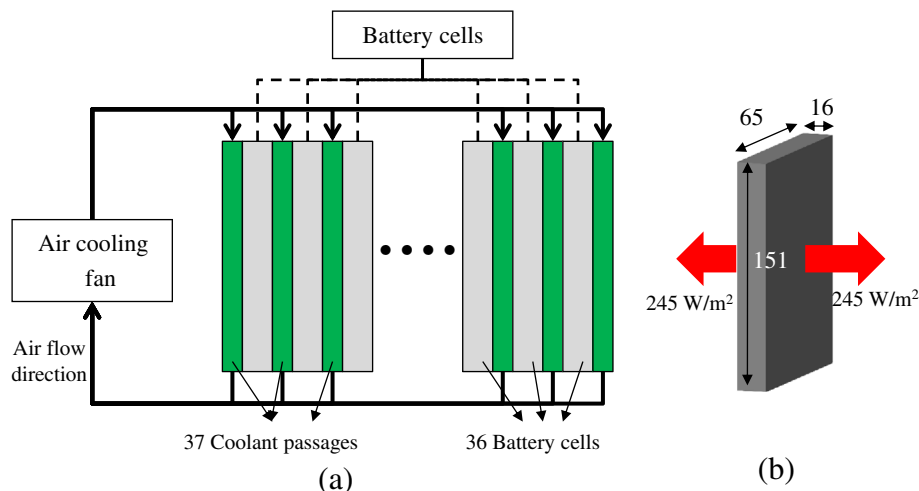


Fig. 1. Schematic diagram of battery system integrated with air coolant passages; (a) battery system, (b) battery cell.

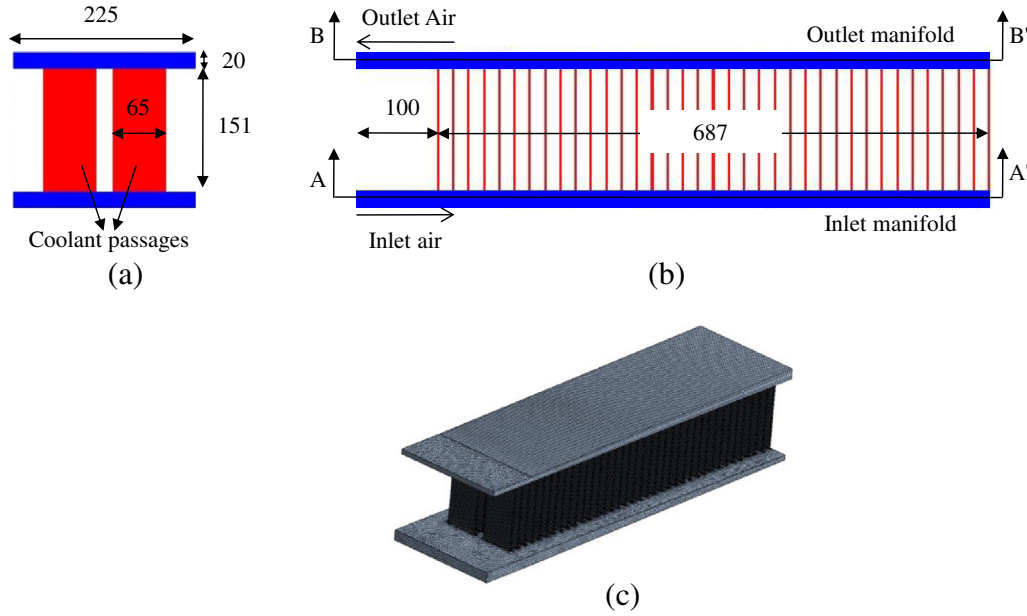


Fig. 2. Cross sectional views of the numerical calculation domain; (a) sectional view, (b) side view, (c) meshed calculation domain.

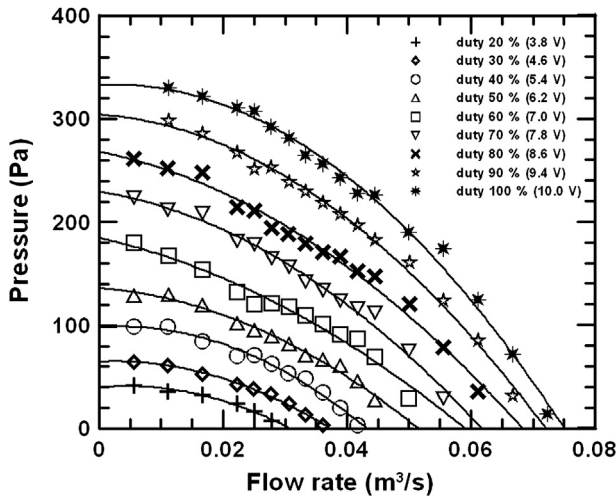


Fig. 3. Characteristic curve of the fan with respect to the power duty.

outlet boundary conditions are used in the numerical calculations. The inlet boundary condition is set to  $0.045 \text{ kg s}^{-1}$  with the temperature of  $40^\circ\text{C}$ , and pressure outlet is fixed at 1 atm. The material properties and heat flux boundary condition are summarized in Table 1.

#### 4. Thermal resistance

The cooling performance of coolant passage can be evaluated by total thermal resistance ( $R_{\text{total}}$ ) which is defined as the ratio of temperature difference between minimum ( $T_{\text{min}}$ ) and maximum ( $T_{\text{max}}$ ) and the applied heat ( $q$ ). The thermal resistance model is useful to classify the heat transfer mechanisms in the cooling system as denoted in Fig. 5, where  $T_i$  and  $T_o$  are the inlet and outlet temperatures, respectively.

$$R_{\text{total}} = \frac{T_{\text{max}} - T_{\text{min}}}{q} \quad (1)$$

The total thermal resistance is the sum of convection ( $R_{\text{con}}$ ) and advection ( $R_{\text{adv}}$ ) thermal resistances. The convection thermal resistance is due to the temperature difference between the air and the coolant passage walls, while advection thermal resistance is caused by the temperature rise at the air cooling due to the heat absorption.

$$R_{\text{total}} = R_{\text{con}} + R_{\text{adv}} \quad (2)$$

$$R_{\text{con}} = \frac{1}{2Ah} \quad (3)$$

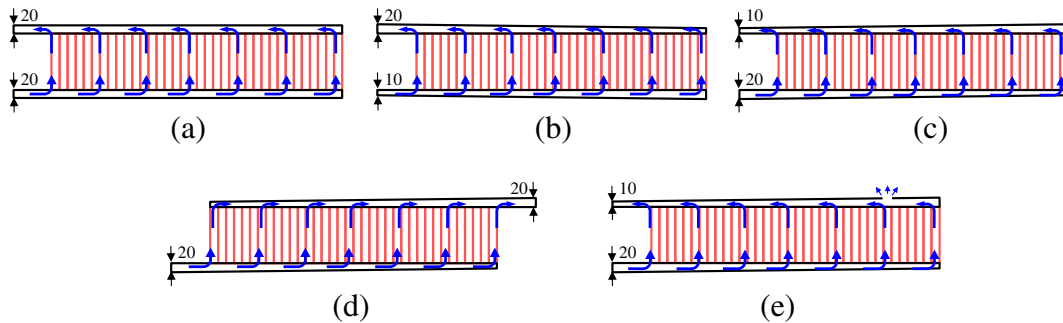
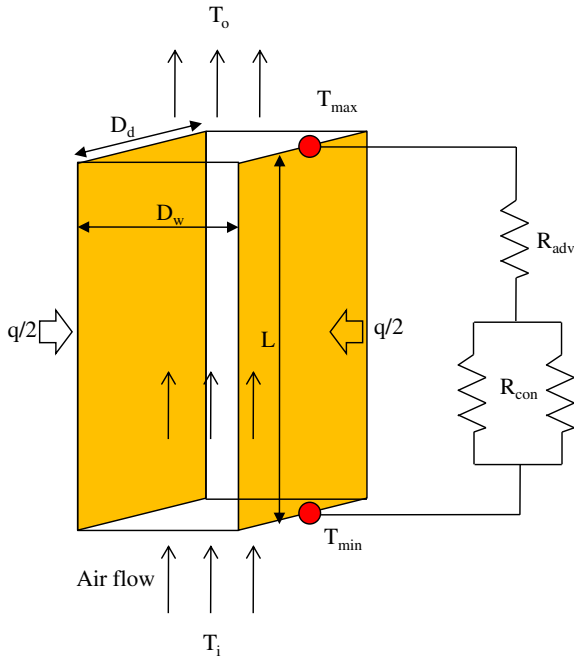


Fig. 4. Geometric configurations of the manifolds; (a) type I, (b) type II, (c) type III, (d) type IV, (e) type V; curved arrows indicate air stream lines.

**Table 1**  
Material properties and heat flux boundary condition.

	Air	Battery cell
Density ( $\text{kg m}^{-3}$ )	1.184	2700
Dynamic viscosity ( $\text{kg m}^{-1} \text{s}^{-1}$ )	$1.98 \times 10^{-5}$	–
Specific heat ( $\text{J kg}^{-1} \text{K}^{-1}$ )	1003	900
Thermal conductivity ( $\text{W m}^{-1} \text{K}^{-1}$ )	435	240
Heat flux ( $\text{W m}^{-2}$ )	–	254



**Fig. 5.** Schematic of thermal resistance model.

$$R_{adv} = \frac{1}{Q \rho_f C_{pf}} \quad (4)$$

where  $A$  and  $h$  are area ( $D_d \times L$ ) and heat transfer coefficient, respectively.  $Q$ ,  $\rho_f$  and  $C_{pf}$  represent flow rate, density, and heat capacity of air, respectively. The heat transfer coefficient can be obtained from the Nusselt number using the following equations:

$$h = \frac{kNu}{D_h} \quad (5)$$

$$D_h = \frac{2D_d D_c}{D_d + D_c}$$

where  $k$ ,  $Nu$ , and  $D_h$  are thermal conductivity of fluid, Nusselt number, and hydraulic diameter, respectively. Assuming a fully-developed temperature profile with constant heat flux, the Nusselt number is expressed in Eq. (6) as a function of geometric parameter ( $G$ ) [22].

$$Nu = -1.047 + 9.326G \quad (6)$$

$$G = \frac{\alpha^2 + 1}{(\alpha + 1)^2}$$

where  $\alpha$  is the channel aspect ratio ( $D_w/D_d$ ). The heat transfer coefficient can be derived with Eqs. (5) and (6), therefore, the convection thermal resistance is calculated with Eq. (3). Finally, the total thermal resistance can be evaluated by using Eqs. (2)–(4).

## 5. Results and discussions

### 5.1. Effect of manifold design

The numerical calculations are performed to predict the temperature distribution under the operating condition and find out the optimum air flow configuration within the design constraints.

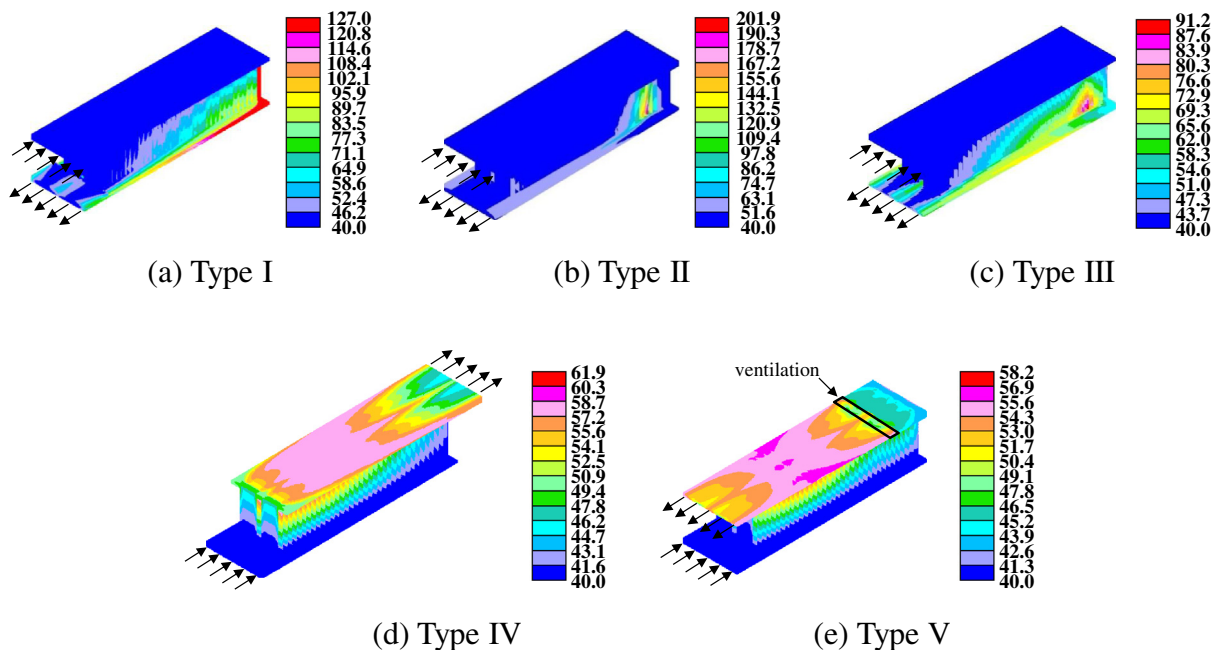


**Fig. 6.** Temperature distributions; (a) type I, (b) type II, (c) type III, (d) type IV, (e) type V.

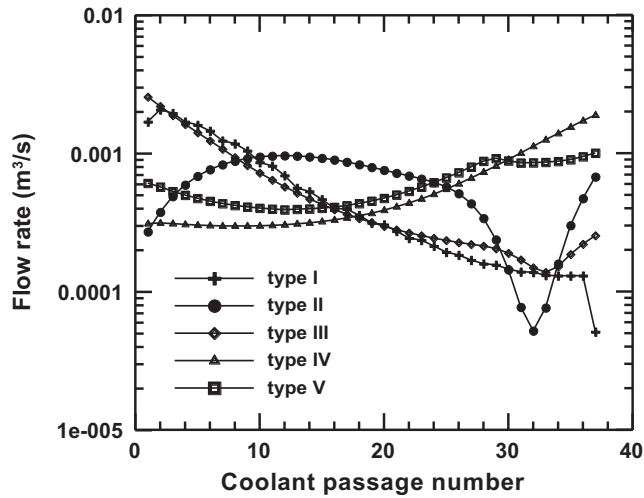


Fig. 7. Air flow rate distributions at the coolant passages for the manifolds.

For convenience, the battery cells and coolant passages are numbered from the air flow inlet region.

Fig. 6(a)–(e) displays the calculated temperature distributions in the five types of manifolds, while the flow rates passing through the coolant passages are plotted in Fig. 7. Comparing Figs. 6 and 7, it can be seen that the maximum temperatures of the battery cells for type I–V directly depend on the air flow rates passing through the coolant passages. For type I, the maximum temperature is calculated to be 127 °C at 37th cell due to the gradual decrease of the air flow rates at the coolant passages, while the expansion shaped manifold in type II causes the maximum temperature to rise up to 201.9 °C of the 31st cell. The improved air flow distribution by employing type III manifold induces lower maximum temperature of 91.2 °C at the 33rd cell which is still beyond the thermal design specification. As the inlet and outlet are positioned on the same side, high pressure is inevitably formed at the 25th–37th coolant passages where the air flow rates is significantly decreased.

Although type IV may not be applicable due to the violation of the given design constraints, the additional numerical calculation is performed to investigate the flow rates and temperature

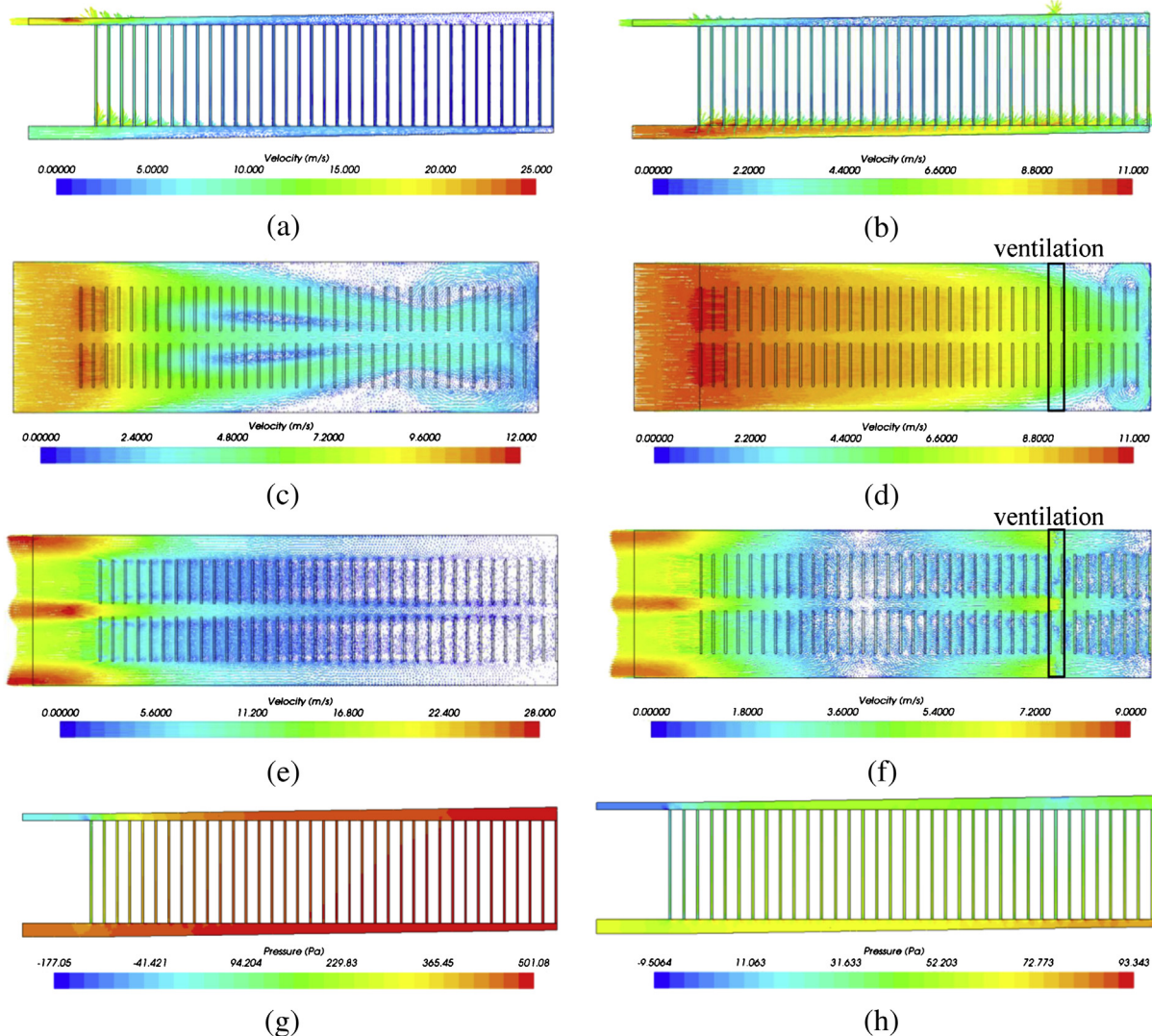


Fig. 8. Velocity and pressure distributions for type III and type V; velocity vectors for (a) type III and (b) type V on the sectional plane of coolant passages, velocity vectors for (c) type III and (d) type V on the top view in the inlet manifold (A–A'), velocity vectors for (e) type III and (f) type V on the top view in the outlet manifold (B–B'), pressure distributions for (g) type III and (h) type V on the sectional plane of coolant passages.

distribution for the purpose of comparison. As displayed in Fig. 6(d), the maximum temperature of battery cell is reduced to be 61.9 °C due to the significantly improved air flow distribution in the coolant passages than type III. It can be seen that relieving the high air pressure at the distant cooling passages from the inlet is significant to achieve the uniform distribution of flow rate and enhanced cooling performance.

Type V is designed based on the type III by adding ventilation which is positioned above the 29th cells with the width of 22 mm. In automotive applications, the battery system is installed in the vehicle with air ventilation to discharge potentially hazardous gases [18,20,21] from the battery. Thus, it is reasonable that the added ventilation in the type V is numerically modelled as a pressure outlet boundary condition. From the calculation result, the maximum temperature is 58.2 °C at the 16th cell as shown in Fig. 6(e), which satisfies the thermal design specification. The changes of air flow velocity and pressure in type V and type III can be seen in Fig. 8. From the comparison between Fig. 8(a) and (b), higher vertical flow velocities in the coolant passages can be found in type V. As the vortices in the inlet manifold of type III are considerably suppressed with the ventilation hole, the more uniform flow velocities in the inlet and outlet manifolds can be obtained as seen in Fig. 8(c)–(f). In Fig. 8(g) and (h), it can be confirmed that the more uniform and lower pressure in the manifolds and coolant passages can also be derived with the ventilation in type V.

The calculated pressure drops for all types of manifolds are summarized in Table 2. It denotes that type I–III are not practically applicable because the calculated pressure drops are beyond the fan operation limit as shown in Fig. 3. In type IV and V, the power consumptions of the fan are estimated to be 47 W and 27 W, respectively. By using the proposed ventilation in type V, the temperature of the battery system can be controlled under thermal design specification cooling performance and with improving energy utilization in HEV application.

## 5.2. Cooling performance

The cooling performance of type V is theoretically analysed. As the Reynolds number are ranged from 920 to 2000 in the coolant passages, the laminar flow assumption is valid for the flow rates obtained from the numerical calculations. The Nusselt number calculated from Eq. (6) is 7.49 and the convection thermal resistance is 1.44 °C W<sup>-1</sup> from the Eqs. (3) and (5). The advection thermal resistances in the coolant passages are simply calculated by using Eq. (3). Fig. 9 displays the theoretically and numerically calculated thermal resistances in the coolant passages. Although the discrepancies of the total thermal resistances between the theoretical and numerical calculations are presented due to the heat transfer by the vortices in the manifold region, theoretical calculation results are in good accordance with the numerical calculation results. For the maximum thermal resistance, the advection thermal resistance is 2.4 °C W<sup>-1</sup> while the convection thermal resistance is 1.44 °C W<sup>-1</sup>. In this regard, the cooling performance can be assessed by the two heat transfer mechanisms. In order to investigate the effects of advection and convection thermal resistances on the cooling performances, a single coolant passage is

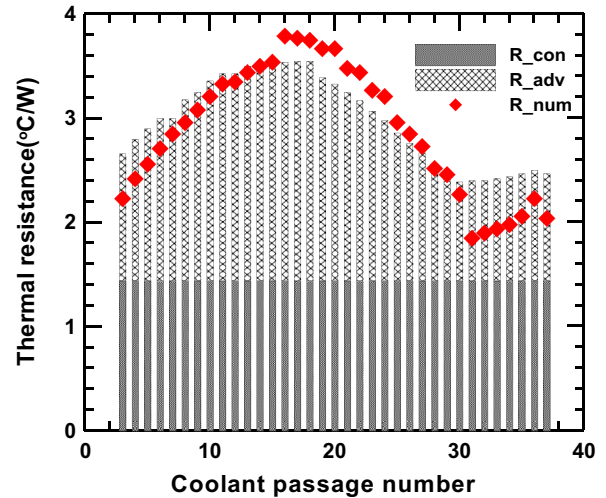


Fig. 9. Thermal resistances derived from theoretical and numerical calculations.

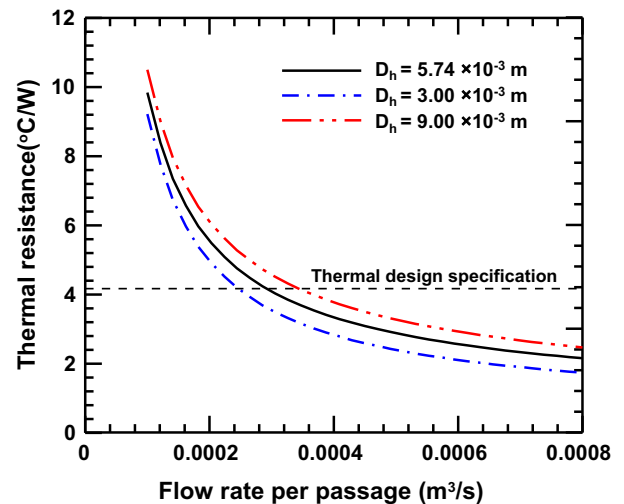


Fig. 10. Thermal resistance versus flow rate and hydraulic diameter.

considered. The maximum thermal resistances are theoretically calculated and displayed in Fig. 10. It is seen that the cooling performances are estimated for the given hydraulic diameters ( $D_h$ ) and coolant flow rates ( $Q$ ). Although smaller hydraulic diameter with higher coolant flow rate improve the cooling performance, the parasitic power for operating fan will increase due to the higher flow resistance.

## 6. Conclusion

In the HEVs, a forced air cooling for the battery system is a preferred option due to compactness, low cost, and design flexibility. This study has introduced the design of air flow configuration for cooling the battery system by conducting numerical calculations. The cooling performance is analysed by adopting the thermal resistance model that can classify the heat transfer mechanisms. Considering the constraints for the air flow configuration, the required cooling performance is achieved by employing the proposed tapered manifold and pressure relief ventilation. The power consumption for operating fan is also improved due to air pressure relief. It is expected that the approach in this study will provide a design guideline for the battery cooling system in the HEVs, electric vehicles, and fuel cell electric vehicles.

**Table 2**  
Summary of the numerical calculation results for the designed samples.

	Type I	Type II	Type III	Type IV	Type V
$\Delta P$ (Pa)	435	441	503	176	64.8
$\Delta T$ (°C)	87	161.9	51.2	21.9	18.2

## References

- [1] J. Xun, R. Liu, K. Jiao, J. Power Sources 223 (2013) 47–61.
- [2] M.R. Giuliano, S.G. Advani, A.K. Prasad, J. Power Sources 196 (2011) 6517–6524.
- [3] M.R. Giuliano, A.K. Prasad, S.G. Advani, J. Power Sources 216 (2012) 345–352.
- [4] T. Tamura, T. Hachida, K. Yoshida, N. Tachikawa, J. Power Sources 195 (2010) 6095–6100.
- [5] Q. Wang, P. Ping, X. Zhao, G. Chu, J. Sun, C. Chen, J. Power Sources 208 (2012) 210–224.
- [6] R. Kizilel, R. Sabbah, J.R. Selman, S. Al-Hallaj, J. Power Sources 194 (2009) 1105–1112.
- [7] C. Zhu, X. Li, L. Song, L. Xiang, J. Power Sources 223 (2013) 155–164.
- [8] K.S. Hariharan, J. Power Sources 227 (2013) 171–176.
- [9] L. Cai, R.E. White, J. Power Sources 196 (2011) 5985–5989.
- [10] Y. Ye, Y. Shi, N. Cai, J. Lee, X. He, J. Power Sources 199 (2012) 227–238.
- [11] R. Mahamud, C. Park, J. Power Sources 196 (2011) 5685–5696.
- [12] C.W. Park, A.K. Jaura, SAE Technical Paper, 2003, 2003-01-2286.
- [13] G. Karimi, X. Li, Int. J. Energy Res. (2012), <http://dx.doi.org/10.1002/er.1956>.
- [14] K. Yeow, H. Teng, M. Thelliez, E. Tan, SAE Int. J. Alt. Power 1 (2012) 65–78.
- [15] Y. Li, H.Q. Xie, J. Li, Appl. Mech. Mater. 271 (2012) 182–185.
- [16] Z. Rao, S. Wang, M. Wu, Z. Lin, F. Li, Energy Convers. Manage. 65 (2013) 92–97.
- [17] R. Sabbah, R. Kizilel, J.R. Selman, S. Al-Hallaj, J. Power Sources 182 (2008) 630–638.
- [18] Z. Rao, S. Wang, Renew. Sustain. Energy Rev. 15 (2011) 4554–4571.
- [19] M.S. Wu, K.H. Liu, Y.Y. Wang, C.C. Wan, J. Power Sources 109 (2002) 160–166.
- [20] A.A. Pesaran, Battery Thermal Management in EVs and HEVs: Issues and Solutions, in: Advanced Automotive Battery Conference, Nevada, Las Vegas, 6–8 February 2001.
- [21] G.L.F. Kitanoski, C. Kussmann, SAE Technical Paper, 2007, 2007-01-3483.
- [22] A. Bejan, Convection Heat Transfer, Wiley, 1990.